13. M. Fernández-Barciela, P.J. Tasker, Y. Campos-Roca, M. Demmler, H. Massler, E. Sanchez, M.C. Curras-Francos, and M. Schlechtweg, A simplified broadband large signal non quasi-static table-based FET model, IEEE Trans Microwave Theory Tech 48 (2000), 395–405.
14. R. Sung, P. Bendix, and M.B. Das, Extraction of high-frequency equivalent circuit parameters of submicron gate-length MOSFET's, IEEE Trans Electron Devices 55 (1998), 1769–1775.
15. G. Crupi, D.M.M.-P. Schreurs, A. Caddemi, A. Raffo, and G. Vannini, Investigation on the non-quasi-static effect implementation for millimeter-wave FET models, Int J RF Microwave Comput-Aided Eng 20 (2010), 87–93.
16. T.M. Martin-Guerrero, A. Santarelli, and C. Camacho-Penalosa, Experimental research into non-quasi-static phenomena in monolithic pHEMT devices, In: 2009 European Microwave Conference, Rome, Italy, October 2009, pp. 1800–1803.
17. G. Gonzalez, Microwave transistor amplifiers analysis and design, Prentice-Hall, NJ, USA, 1996.
18. A. Caddemi, G. Crupi, and A. Macchiarella, On wafer scaled GaAs HEMTs: Direct and robust small signal modelling up to 50 GHz, Microwave Opt Technol Lett 51 (2009), 1958–1963.
19. G. Crupi, G. Avolio, A. Raffo, P. Barmuta, D.M.M.-P. Schreurs, A. Caddemi, and G. Vannini, Investigation on the thermal behavior for microwave GaN HEMTs, Solid-State Electron 64 (2011), 28–33.
20. A. Raffo, V. Vadalà, D.M.M.-P. Schreurs, G. Crupi, G. Avolio, A. Caddemi, and G. Vannini, Nonlinear dispersive modeling of electron devices oriented to GaN power amplifier design, IEEE Trans Microwave Theory Tech 58 (2010), 710–718.
21. G. Crupi, A. Raffo, D.M.M.-P. Schreurs, G. Avolio, V. Vadalà, S. Di Falco, A. Caddemi, and G. Vannini, Accurate GaN HEMT non-quasi-static large-signal model including dispersive effects, Microwave Opt Technol Lett 53 (2011), 692–697.
22. A. Caddemi, A. Di Paola, M. Sannino, Microwave noise parameters of HEMTs vs. temperature by a simplified measurement procedure, In: Proceedings of the 4th International Workshop on High Performance Devices for Microwave and Optoelectronic Applications, Leeds, UK, November 1996, pp. 153–157.



# DUAL-BAND PRINTED DIPOLE ANTENNA WITH WIDE BEAMWIDTH FOR WLAN ACCESS POINTS

**Son Xuat Ta,[1] Jea Jin Han,[1,2] Hosung Choo,[3] and Ikmo Park[1]**
[1] School of Electrical and Computer Engineering, Ajou University, 5 Woncheon-dong, Youngtong-gu, Suwon 443-749, Korea; Corresponding author: ipark@ajou.ac.kr
[2] Danam Systems, 799 Gwangyang2-dong, Dongan-gu, Anyang 431-767, Korea
[3] School of Electronics and Electrical Engineering, Hongik University, 72-1 Sangsu-dong, Mapo-gu, Seoul 121-791, Korea

*Received 20 March 2012*

**ABSTRACT:** *In this article, we propose a dual-band angled printed dipole antenna with wide beamwidth for use in the access points of wireless local area network operating in the 2.4- and 5-GHz bands. The antenna is fed by a novel integrated balun consisting of a curved microstripline and a circular slot for broadband operation. An angled dipole and two vertical copper plates on the ground plane are used to achieve wide beamwidth in the lower and upper bands, respectively.*
 Microwave Opt Technol Lett 54:2806–2811, 2012; View this article online at wileyonlinelibrary.com.
DOI 10.1002/mop.27176

**Key words:** *WLAN; access point; angled dipole; dual-band; wide beamwidth*

## 1. INTRODUCTION

Wireless local area networks (WLANs) in the 2.4-GHz (2.4–2.485 GHz) and 5-GHz (5.15–5.35 GHz, 5.47–5.725 GHz, and 5.725–5.875 GHz) bands have been widely used in recent years. Because of the existence of many shadowing areas within a given network range, a large number of access points (APs) are needed to be installed to achieve pervasive coverage of WLAN systems. To provide such pervasive WLAN coverage, the antennas used for APs (which are commonly mounted on the walls or ceilings of rooms) must radiate signals in such a manner that the radiated electromagnetic (EM) wave is relatively the same anywhere in the room; further, the back radiation from an antenna needs to be insignificant. Thus, the antenna for an AP not only requires dual-band operation but also needs to have a radiation profile with similar gain, wide beamwidth, and high front-to-back ratio in both bands. Various kinds of antennas have been used for WLAN APs for single-band [1–2], dual-band [3], switchable-band [4], and wideband [5] operations. However, most of these antennas essentially address bandwidth improvement and impedance matching optimization; the study of the radiation patterns of the antennas has thus far been neglected.

In this article, we introduce a dual-band printed dipole antenna that has nearly identical radiation patterns with similar gain and beamwidth in both the 2.4- and 5-GHz WLAN bands. Our antenna utilizes two techniques to improve the radiation pattern; these techniques include the use of an angled dipole and vertical copper plates arranged on the ground plane for improvement in the radiation pattern of the lower and upper bands, respectively.

## 2. ANTENNA DESIGN AND CHARACTERISTICS

Figure 1 shows the geometry of a dual-band printed dipole antenna. The antenna is composed of two printed dipoles, two copper plates, an integrated balun feed, and a ground plane. The ground plane comprised a rectangular plate with a thickness of 0.2 mm and width and length of $70 \times 60$ mm$^2$, respectively. The printed dipole and balun were designed on the front and back surfaces of a Rogers RO4003 substrate with a relative dielectric constant of 3.38 and a thickness of 0.508 mm. The trapezoidal-shaped substrate had a width and height of $W_{sub} = 60$ mm and $H_{sub} = 24$ mm, respectively. The two dipoles printed on the substrate were welded on the ground plane. The large dipole was angled at $\theta$ degrees to the horizontal, as shown in the figure. The initial lengths of the two printed dipoles ($L_1$ and $L_2$) were chosen as approximately half the effective wavelength ($\lambda_{eff}/2$) for both the 2.45- and 5.5-GHz bands. The balun consisted of a curved microstripline and a circular slot. The curved microstripline comprised of a 50-Ω feedline and a half ring, both with a width of $w_{ms} = 1.14$ mm. The circular slot was etched on the printed dipoles. The radii of the ring and circular slot were $r_1 = 2$ mm and $r_2 = 2.86$ mm, respectively. The antenna was fed by an SMA 50-Ω coaxial connector. The inner conductor of the coaxial connector was extended through the ground plane and connected to the 50-Ω microstripline. On the ground plane, two vertical copper plates whose width and height were $W_p$ and $H_p$, respectively, were arranged symmetrically over the substrate with a spacing of $S_p$.

A full-wave EM simulator (Microwave Studio, Computer Simulation Technology) was used to design the antenna. From the EM simulation, the following design parameters were found to achieve similar gain and wide beamwidth in both the $E$- and $H$-plane patterns at the 2.4- and 5-GHz bands: $g = 0.6$ mm,

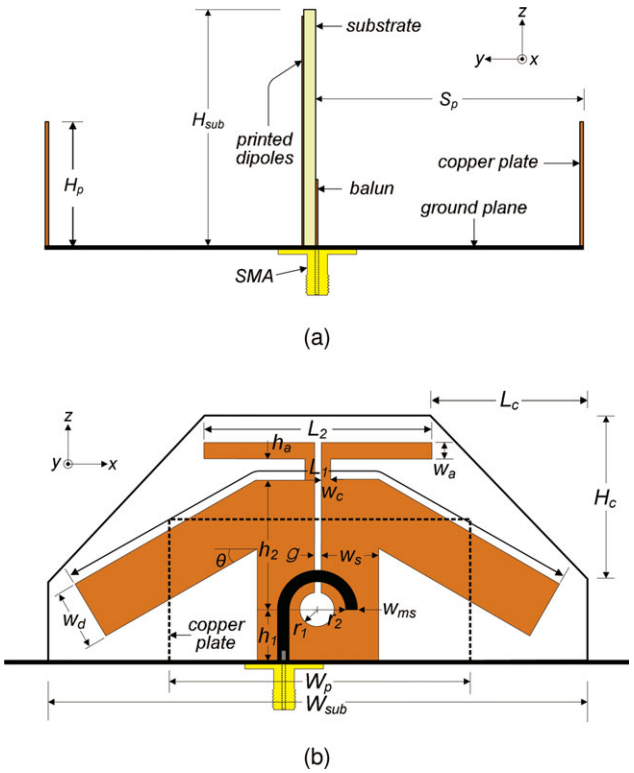


**Figure 1** Geometry of dipole antenna: (a) side view and (b) front view. [Color figure can be viewed in the online issue, which is available at wileyonlinelibrary.com]

$h_1 = 5$ mm, $h_2 = 14$ mm, $h_a = 2$ mm, $L_1 = 60.4$ mm, $L_2 = 23.4$ mm, $r_1 = 2$ mm, $r_2 = 2.86$ mm, $H_p = 15$ mm, $H_{sub} = 24$ mm, $H_c = 17$ mm, $\theta = 30°$, $w_a = 2$ mm, $w_c = 0.6$ mm, $w_d = 6$ mm, $w_s = 5.7$ mm, $w_{ms} = 1.14$ mm, $W_p = 34$ mm, $W_{sub} = 60$ mm, $S_p = 30$ mm, and $L_c = 18$ mm. Based on the above optimized design parameters, we investigated the corresponding variation in the antenna characteristics due to change in the main design parameters. Figure 2 shows the simulated reflection coefficient of the antenna as a function of frequency for different lengths of the large dipole, $L_1$. As the length $L_1$ was increased

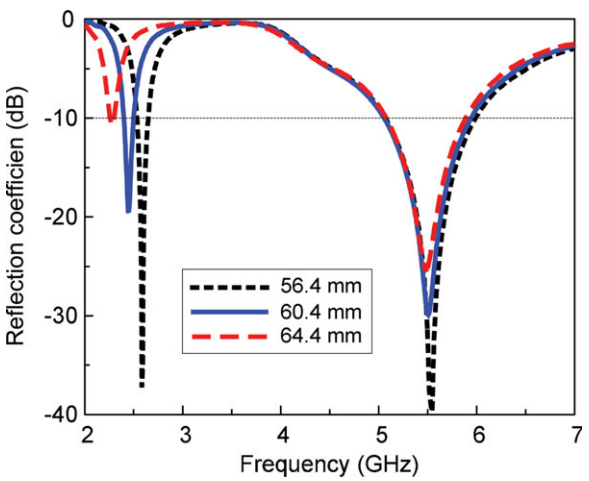


**Figure 2** Reflection coefficient as function of frequency for different values of $L_1$. [Color figure can be viewed in the online issue, which is available at wileyonlinelibrary.com]

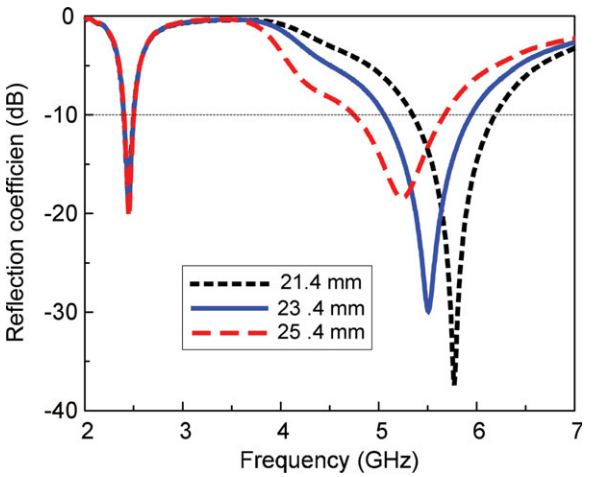


**Figure 3** Reflection coefficient as function of frequency for different values of $L_2$. [Color figure can be viewed in the online issue, which is available at wileyonlinelibrary.com]

from 56.4 to 64.4 mm in increments of 4 mm, the lower resonant frequency decreased while the upper one changed slightly. This indicates that the length of the large dipole mainly determines the lower resonant frequency. Figure 3 shows the simulated reflection coefficient of the antenna as a function of frequency for different lengths of the small dipole, $L_2$. As the length $L_2$ was increased from 21.4 to 25.4 mm in increments of 2 mm, the upper resonant frequency decreased while the lower resonance remained unchanged. This indicates that the length of the small dipole mainly determines the upper resonant frequency.

The $E$-plane pattern of a printed dipole can be controlled using an angled dipole. This can be observed in Figure 4, which plots the 2.45-GHz patterns of the antenna for various values of the angle $\theta$ of the large dipole. As $\theta$ was increased from 0° to 30° in increments of 15°, the $E$-plane pattern widened while the H-plane pattern changed slightly. In both cases, the peak gain decreased; however, the front-to-back ratio improved. In addition, a $\theta$ setting of 30° offered nearly the same 3-dB beamwidth in the $E$- and $H$-planes. In the 2.4-GHz band, the effect of the dipole angle variation on the reflection coefficient is negligible, and hence, this relationship curves not shown here.

As mentioned above, two vertical copper plates are arranged symmetrically at the edge of the ground plane for improving the radiation pattern of the antenna in the upper frequency band. The effect of using the copper plates is observed in Figures 5–7, which show the 5.5-GHz patterns of the antenna for various values of the copper plate height ($H_p$), width ($W_p$), and spacing between the copper plate and substrate ($S_p$), respectively. In the trials corresponding to Figures 5 and 6, as $H_p$ and $W_p$ were varied from 0 to 30 mm in 15 mm steps and from 14 to 54 mm in 20 mm steps, respectively; the $E$-plane pattern changed slightly while the $H$-plane pattern narrowed and the peak gain increased. As shown in Figure 7, the spacing value of $S_p = 30$ mm led to the optimized 5.5-GHz pattern in terms of similar radiation pattern with a wide beamwidth in both the $E$- and $H$-planes. These results indicate that the parameters $H_p$, $W_p$, and $S_p$ mainly control the $H$-plane pattern at the 5-GHz band. The copper plates are designed for control of the radiation pattern in the upper band only, and their effects on other antenna characteristics are insignificant.

An Agilent N5230A network analyzer and a 3.5-mm coaxial calibration standard GCS35M were used for the measurements

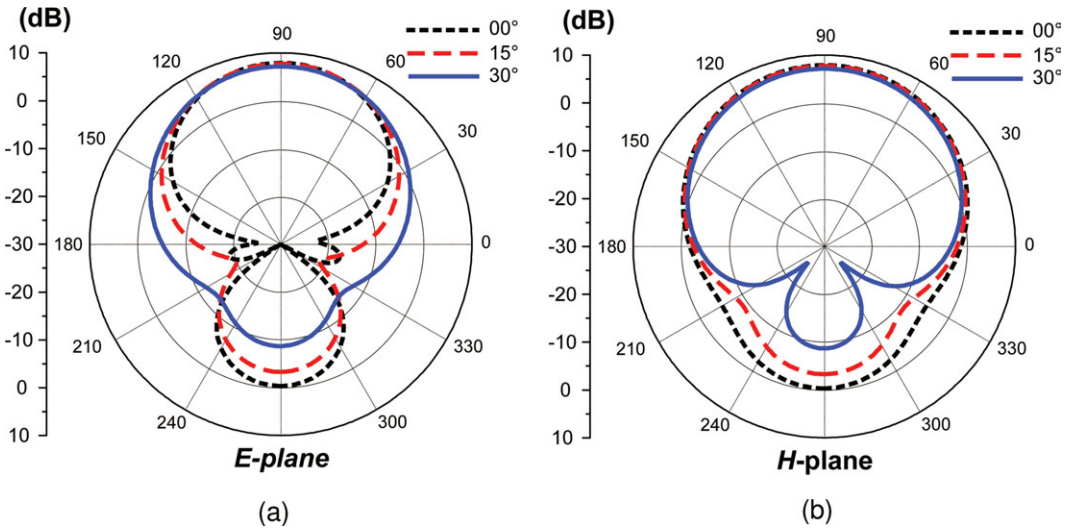


**Figure 4** Radiation pattern at 2.45 GHz for different values of $\theta_1$: (a) *E*-plane and (b) *H*-plane. [Color figure can be viewed in the online issue, which is available at wileyonlinelibrary.com]

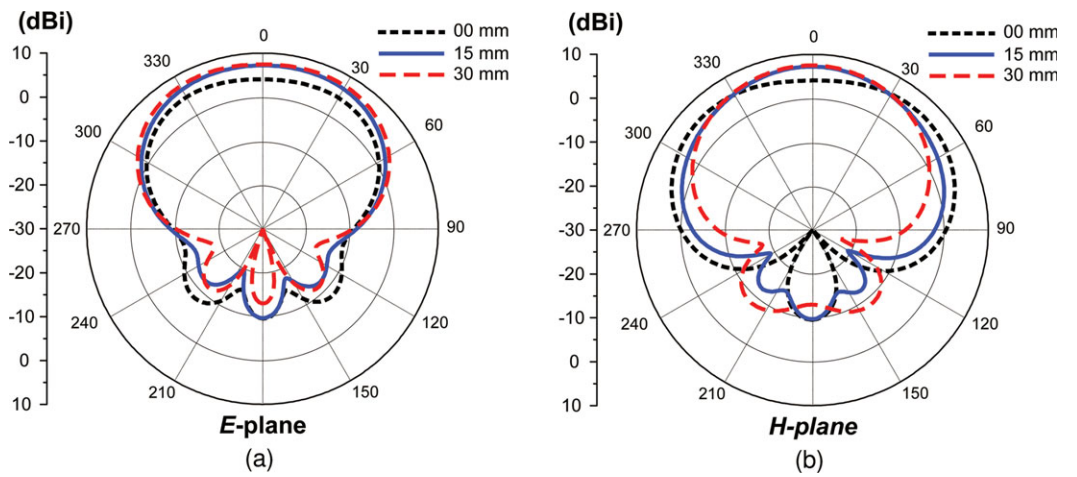


**Figure 5** Radiation pattern at 5.5 GHz for different values of $H_p$: (a) *E*-plane and (b) *H*-plane. [Color figure can be viewed in the online issue, which is available at wileyonlinelibrary.com]

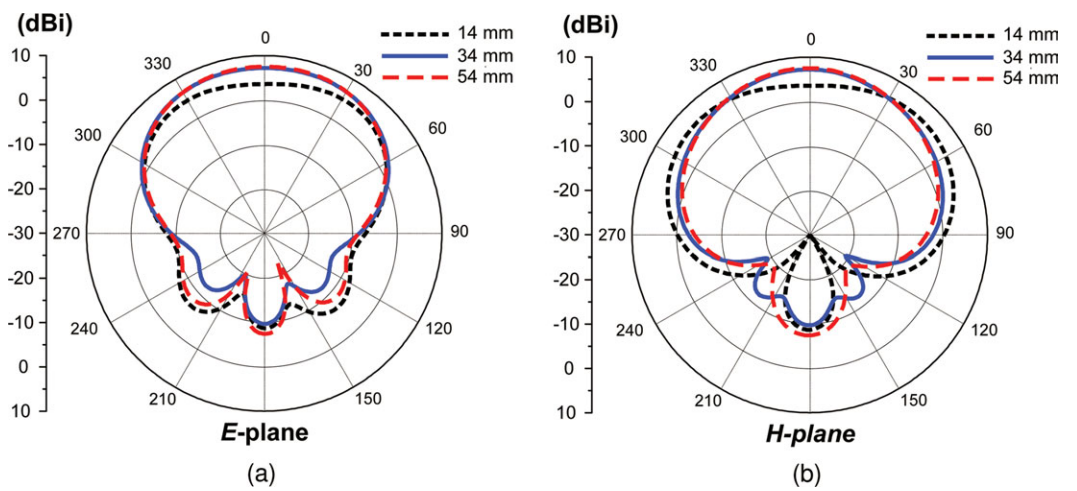


**Figure 6** Radiation pattern at 5.5 GHz for different values of $W_p$: (a) *E*-plane and (b) *H*-plane. [Color figure can be viewed in the online issue, which is available at wileyonlinelibrary.com]

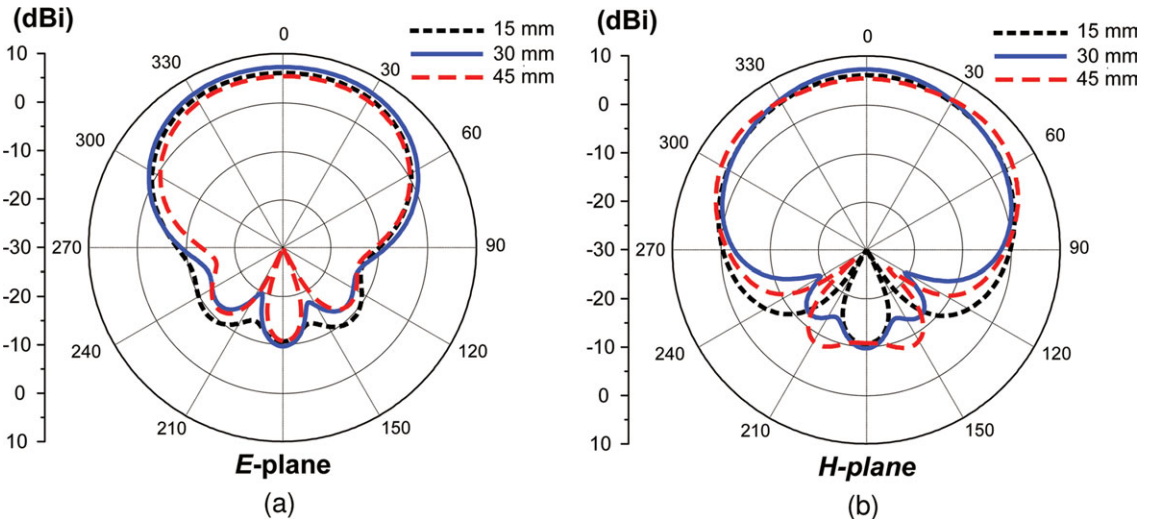


**Figure 7** Radiation pattern at 5.5 GHz for different values of $S_p$: (a) *E*-plane and (b) *H*-plane. [Color figure can be viewed in the online issue, which is available at wileyonlinelibrary.com]

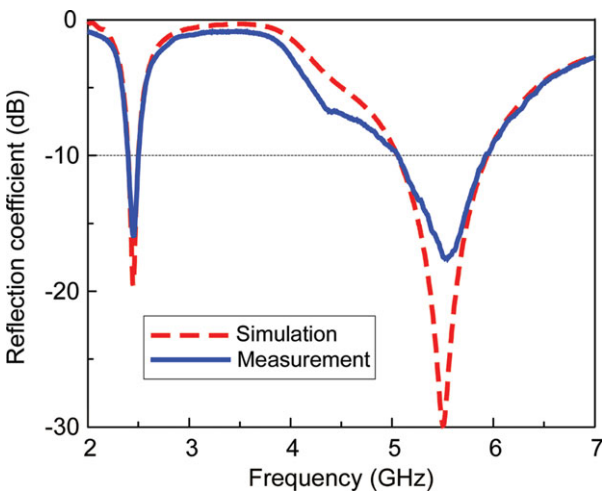


**Figure 8** Reflection coefficient of antenna. [Color figure can be viewed in the online issue, which is available at wileyonlinelibrary.com]

of the antenna prototype. As shown in Figure 8, the measured and simulated reflection coefficients of the antenna agreed rather closely. The measured impedance bandwidths were 2.39–2.5 GHz and 5.05–5.92 GHz for the −10 dB reflection coefficient, while the simulated bandwidths ranged from 2.4 to 2.5 GHz and 5.05 to 5.94 GHz. The slight discrepancy between the measurement and the simulation could be attributed to misalignment of the balun.

The 2.45-, 5.2-, 5.5-, and 5.8-GHz radiation patterns of the antenna are shown in Figures 9–12, respectively. As observed from the figures, the measurements and simulations show good agreement. At 2.45 GHz, the measured radiation patterns showed a front-to-back ratio of 23.5 dB, cross-polarization level of less than −19 dB, and half-power beamwidths (HPBWs) of 100° and 111° in the *E*- and *H*-planes, respectively. At 5.2 GHz, the measured radiation patterns showed a front-to-back ratio of 27.8 dB, cross-polarization level of less than −13.4 dB, and HPBWs of 116° and 114° in the *E*- and *H*-planes, respectively. At 5.5 GHz, the measured radiation patterns showed a front-to-back ratio of 32.12 dB, cross-polarization level of less than −14.2 dB, and HPBWs of 118° and 110° in the *E*- and

F9-F12

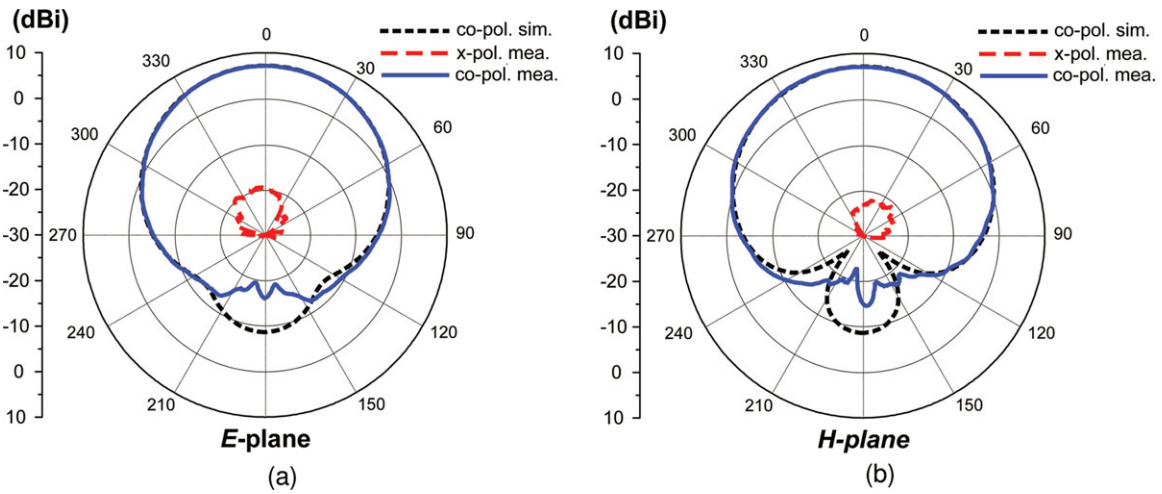


**Figure 9** Radiation patterns of antenna at 2.45 GHz: (a) *E*-plane and (b) *H*-plane. Simulated cross-polarization is excluded because the simulated values are too small to be indicated in the figure. [Color figure can be viewed in the online issue, which is available at wileyonlinelibrary.com]

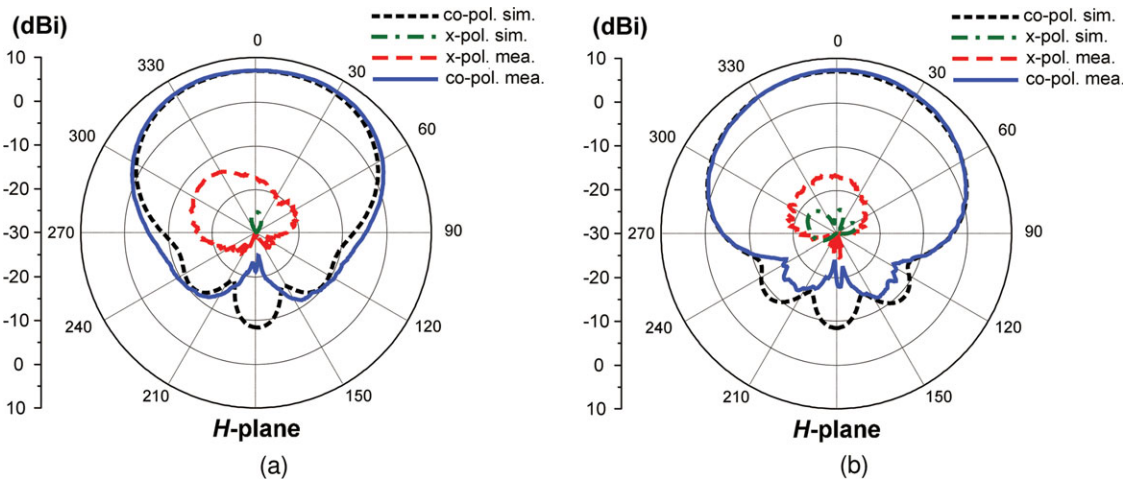


**Figure 10** Radiation patterns of antenna at 5.2 GHz: (a) *E*-plane and (b) *H*-plane. [Color figure can be viewed in the online issue, which is available at wileyonlinelibrary.com]

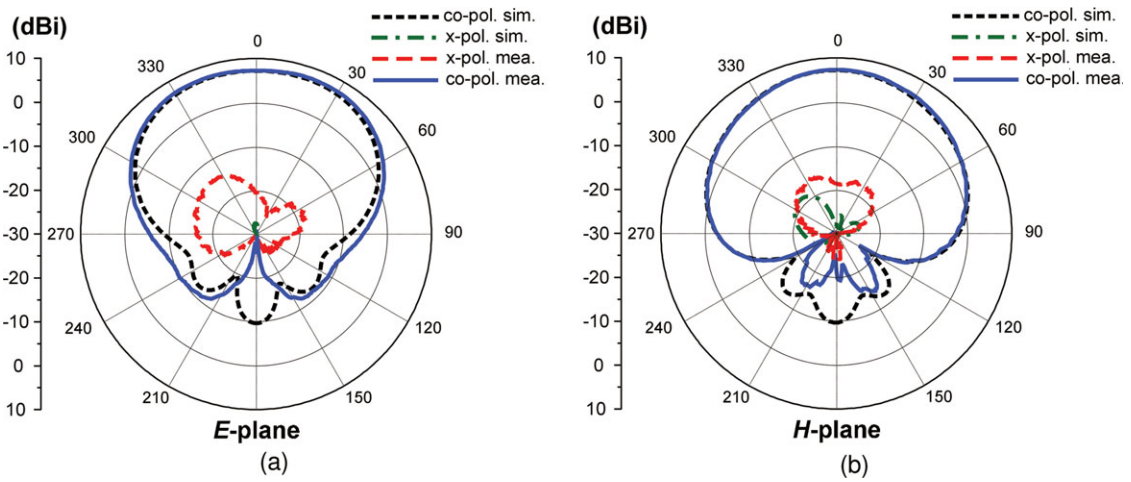


**Figure 11** Radiation patterns of antenna at 5.5 GHz: (a) *E*-plane and (b) *H*-plane. [Color figure can be viewed in the online issue, which is available at wileyonlinelibrary.com]

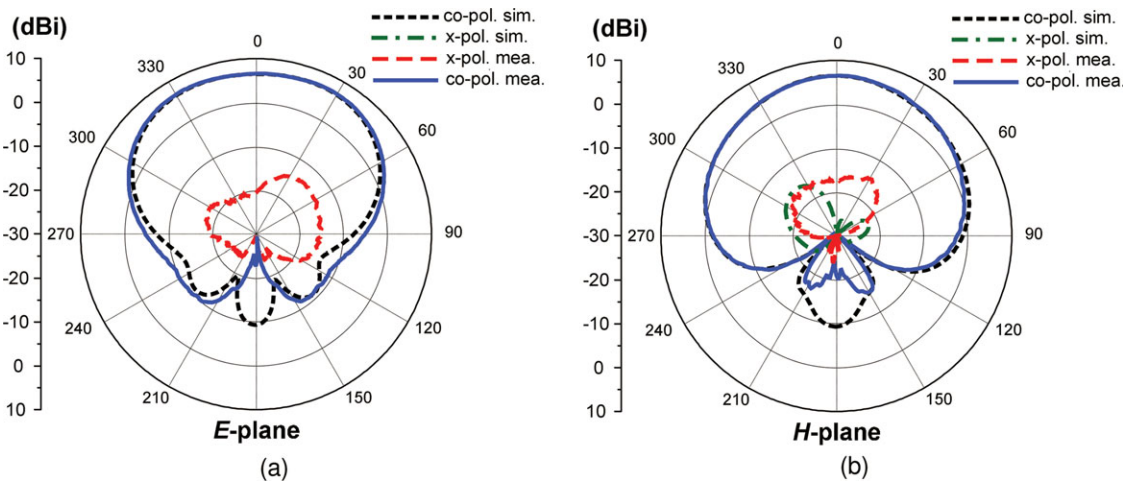


**Figure 12** Radiation patterns of antenna at 5.8 GHz: (a) *E*-plane and (b) *H*-plane. [Color figure can be viewed in the online issue, which is available at wileyonlinelibrary.com]

*H*-planes, respectively. At 5.8 GHz, the measured radiation patterns showed a front-to-back ratio of 29.44 dB, cross-polarization level of less than −13.6 dB, and HPBWs of 120° and 113° in the *E*- and *H*-planes, respectively. The measured gains are 7.11, 7.02, 7.14, and 6.92 dBi at frequencies of 2.45, 5.2, 5.5, and 5.8 GHz, respectively.

### 3. CONCLUSION

Our study proposed the use of a printed dipole antenna for the 2.4- and 5-GHz WLAN APs. The angled dipole and two vertical copper plates arranged on the ground plane were used to achieve similar gain and beamwidth in the lower and upper bands, respectively. The antenna yielded a bandwidth of 2.39–2.5 GHz and 5.05–5.92 GHz for the −10 dB reflection coefficient. The radiation pattern of antenna showed wide beamwidth, high front-to-back ratio, and similar gain for both the lower and upper bands. With the obtained wide beamwidth and similar gain in the 2.4- and 5-GHz bands, the proposed antenna could be stably operated in a dual-band WLAN.

### REFERENCES


1. R. Gardelli, G.L. Cono, and M. Albani, A low-cost suspended patch antenna for WLAN access points and point-to-point links, IEEE Antenna Wireless Propagat Lett 3 (2004), 90–93.
2. T.G. Ma, C.W. Wang, R.C. Hua, and J.W. Tsai, A modified quasi-Yagi antenna with a new compact microstrip-to-coplanar strip transition using artificial transmission lines, IEEE Trans Antennas Propagat 57 (2009), 2469–2474.
3. G. Augustin, S.V. Shynu, C.K. Aanandan, and K. Vasudevan, Compact dual-band antenna for wireless access point, Electron Lett 42 (2006), 502–503.
4. M.R. Hamid, P.S. Hall, P. Gradner, and F. Ghanem, Switched WLAN-wideband tapered slot antenna, Electron Lett 46 (2010), 523–524.
5. C.R. Medeiros, E.B. Lima, J.R. Costa, and C.A. Fernandes, Wideband slot antenna for WLAN access point, IEEE Antenna Wireless Propagat Lett 9 (2010), 79–82.




# LOW-PROFILE CIRCULARLY POLARIZED GNSS ANTENNA

**M. Silva Pimenta, F. Ferrero, R. Staraj, and J.M. Ribero**
Laboratoire d'Electronique, Antennes et Télécommunications, CREMANT, Université de Nice-Sophia Antipolis, UMR 7248, CNRS Bât.4, 250 rue Albert Einstein, 06560 Valbonne, France;
Corresponding author: spimenta@unice.fr

*Received 20 March 2012*

**ABSTRACT:** *In this article, we present a low-profile and low cost antenna for GPS ($L_1$–$L_2$–$L_5$), Galileo ($E_5$–$E_1$–$E_2$), and Glonass ($G_1$–$G_2$) standard. This antenna is a dual-feed planar patch antenna with four slots to achieve dual-band operation. The radiating element is fed by a wideband 90° quadrature hybrid coupler to obtain circular polarization on the both bands. The quadrature feeding is achieved using a three-branch-line hybrid coupler. The return loss bandwidth of the system ($S_{11} \leq -10$ dB) is 22% in the lower band and 14% in the upper one. The axial ratio (AR) bandwidth in broadside direction (AR= 3 dB) is 20% in the lower band and 11.3% at the upper one. The antenna gain is 6 and 8.4 dBi in the normal direction at the central frequency of 1.23 and 1.6 GHz, respectively. The total dimensions of the antenna are 170 mm$^2$ with a thickness of 7.524 mm.* © 2012 Wiley Periodicals, Inc.
Microwave Opt Technol Lett 54:2811–2814, 2012; View this article online at wileyonlinelibrary.com. DOI 10.1002/mop.27175

**Key words:** *global navigation satellite systems antenna; three-branch-lines hybrid coupler; dual-band antenna; slotted patch; circular polarization*

### 1. INTRODUCTION

Several satellite navigation systems have been and are being developed around the world. Global navigation satellite systems (GNSS), provides reliable positioning in real time. The GNSS includes GPS (USA), Compass (PR China), GLONASS (Russia), and currently Galileo, with the arrival of the own Europe GNSS. Multiband GNSS antennas having compact size, lightweight, and low cost are needed for GNSS receivers on small satellites, air planes, ships, and mobile terminals on the ground [1–2].

A lot of solutions have been proposed in literature to design dual-band circularly polarized antennas. Two main techniques exist: the first one uses stacked truncated corner patch to create dual-band circular operations. This solution is interesting but the thickness of the antenna is generally large [3]. The second technique, used in this article, consists in using a square patch on a single substrate layer, having rectangular slots etched in the metallization of the radiating element to produce dual-band operation [4–6]. The technique uses in this kind of structure, presented in Ref. 7, consists in exciting the two modes $TM_{100}$ and $TM_{300}$ of the patch. Then, to generate the circular polarization, two main solutions exist. The first one consists in creating some degenerated mode by adding some dissymmetry on the patch. For example, in Ref. 8 to obtain a GPS $L_1$–$L_2$ bands antenna, the authors used a truncated patch with a simple feed. However, the drawback of this method is the limitation of the axial ratio (AR) bandwidth. The second solution is to feed two orthogonal modes with an equal amplitude and a quadrature of phase, thus the AR bandwidth is only depending on the quadrature feeding circuit. In Ref. 9, the author have a wideband circular polarization antenna using double square stacked patch with a capacitive feeding and a power splitter using metamaterials lines, this work is interesting but the antenna is two thick. To generate wideband quadrature feeding, several solutions have been proposed in the literature. Reference 10 demonstrates the possibilities of the right-handed left-handed transmission lines to design a dual-band hybrid quadrature coupler, combining surface-mounted elements with planar transmission lines. Tseng and Chang [11] proposed a power splitter using composite right-left handed transmission lines, with a Wilkinson power divider and two phase-adjusting transmission lines. An impressive bandwidth of 300% is obtained with an amplitude imbalance lower than 0.5 dB and a phase error lower than 5°. However, this metamaterial coupler is not robust to load mismatch. Equal power splitting and phase quadrature are not satisfied if the load impedance is different from 50 Ω. Dual band hybrid couplers [12] are applicable in the GPS bands if the center frequency of the hybrid coupler is well chosen because the frequency ratio is only about 1.31. This solution is simple to implement and does not need any lumped element.

### 2. ANTENNA DESIGN

#### *2.1. Dual-Band Slotted Patch Antenna with Dual-Feed*

The antenna is a slotted square patch with a dual-feed for circular polarization. The dual-band operation is achieved with slots etched and well placed in the patch, the circular polarization is obtained with a dual-feed in quadrature of phase. The two modes $TM_{100}$ and $TM_{300}$ of the patch are exited to have similar radiation pattern properties with no nulls on the broadside direction. The antenna is printed over a 0.127-mm thick duroid